⌘ *Author's Choice*

THE JOURNAL OF BIOLOGICAL CHEMISTRY VOL. 286, NO. 18, pp. 16392–16401, May 6, 2011

The Catalytic Architecture of Leukotriene C_4 Synthase with Two Arginine Residues*[S]

Received for publication, June 1, 2010, and in revised form, January 17, 2011 Published, JBC Papers in Press, March 16, 2011, DOI 10.1074/jbc.M110.150177

Hiromichi Saino[‡1], Yoko Ukita[‡1], Hideo Ago[‡1,2], Daisuke Irikura[‡], Atsushi Nisawa[§], Go Ueno[§], Masaki Yamamoto[§], Yoshihide Kanaoka[¶], Bing K. Lam[¶], K. Frank Austen[¶], and Masashi Miyano[‡3]

From the [‡]Structural Biophysics Laboratory and [§]Research Infrastructure Group, RIKEN SPring-8 Center, Harima Institute, 1-1-1 Kouto, Sayo, Hyogo 679-5148, Japan and the [¶]Department of Medicine, Harvard Medical School and Division of Rheumatology, Immunology, and Allergy, Brigham and Women's Hospital, Boston, Massachusetts 02115

Leukotriene (LT) C_4 and its metabolites, LTD_4 and LTE_4, are involved in the pathobiology of bronchial asthma. LTC_4 synthase is the nuclear membrane-embedded enzyme responsible for LTC_4 biosynthesis, catalyzing the conjugation of two substrates that have considerably different water solubility; that amphipathic LTA_4 as a derivative of arachidonic acid and a water-soluble glutathione (GSH). A previous crystal structure revealed important details of GSH binding and implied a GSH activating function for Arg-104. In addition, Arg-31 was also proposed to participate in the catalysis based on the putative LTA_4 binding model. In this study enzymatic assay with mutant enzymes demonstrates that Arg-104 is required for the binding and activation of GSH and that Arg-31 is needed for catalysis probably by activating the epoxide group of LTA_4.

Leukotriene C_4 (LTC_4)[4] and its metabolites, LTD_4 and LTE_4, are collectively called the cysteinyl leukotrienes (cys-LTs). They are generated by certain bone marrow-derived proinflammatory cells, such as mast cells, eosinophils, basophils, and monocyte-derived tissue cells, including macrophages and dendritic cells (1–5). They have been implicated in the pathobiology of human bronchial asthma for their direct effect as bronchoconstrictors (6, 7) and permeability-enhancing mediators (8, 9), their presence in urine and bronchoalveolar fluid during exacerbations (10, 11), and the clinical efficacy of therapeutic agents interfering with the biosynthesis or receptor-mediated action of the cys-LTs (12, 13). Therapeutic intervention has also been shown to be effective in allergic rhinitis, acute and chronic urticaria, and angioedema (14–16), indicating a critical role for the cys-LTs in a broad range of allergic diseases.

The biosynthetic pathway of the cys-LTs begins with cytosolic phospholipase A_2-dependent release of arachidonic acid from the outer nuclear membrane (17) and its subsequent metabolism to 5-hydroperoxyeicosatetraenoic acid and then LTA_4 by 5-lipoxygenase in the presence of the 5-lipoxygenase activating protein (18–20). LTA_4 is then conjugated with reduced glutathione (GSH) to form LTC_4 by means of LTC_4 synthase (LTC_4S) (21). Both 5-lipoxygenase activating protein and LTC_4S are integral membrane proteins of the nuclear membrane and belong to the membrane-associated proteins in eicosanoid and glutathione metabolism superfamily (22, 23). Intracellular LTC_4 is released by the multidrug resistance protein-mediated, energy-dependent pathway. It undergoes extracellular metabolism to LTD_4 by the cleavage of glutamic acid via γ-glutamyl transpeptidase or γ-glutamyl leukotrienase and then to LTE_4 by removal of glycine by dipeptidases (24, 25). The three sequentially generated cys-LTs differ in extracellular stability such that only LTE_4 is readily detected in urine or at a site of inflammation (26, 27). They are also distinct in their affinity for the cloned receptors $CysLT_1$ and $CysLT_2$ receptors (28, 29). Studies of mice with targeted disruption of LTC_4S have extended the appreciation of the role of cys-LTs in models of inflammation beyond their smooth muscle activity. $LTC_4S^{-/-}$ mice have a marked reduction in antigen-induced allergic pulmonary inflammation and in bleomycin-induced pulmonary fibrosis (30, 31).

An adenosine diphosphate-reactive purinergic ($P2Y_{12}$) receptor was recently reported to be required for LTE_4-dependent pulmonary inflammation (32, 33). In addition, a functional receptor for LTE_4-mediated vascular permeability was observed in mice lacking both the classical $CysLT_1$ and $CysLT_2$ receptors (34). An LTE_4-reactive receptor has been considered likely because LTE_4 has pathophysiological effects on airway inflammation in asthma, such as mucosal eosinophilia and airway hyperresponsiveness, although LTE_4 has a much lower affinity for the established cys-LT receptors.

The previous crystal structure study provided a detailed view of the GSH binding of LTC_4S (35, 36). The GSH binding site is formed at the interface of two adjacent monomers in the LTC_4S trimer. Nine amino acid residues interact directly with the bound GSH, and almost all of these amino acid residues are conserved in the amino acid sequence alignment in the mem-

* This work was supported, in whole or in part, by National Institutes of Health Grants AI31599, HL36110, and HL82695 (to B. K. L.) and HL90630 (to Y. K.). This work was supported in part by a grant-in-aid for Scientific Research in the Global Center of Excellence program (A-12) from the Ministry of Education, Culture, Sports, Science, and Technology of Japan (to H. A.).

[S] The on-line version of this article (available at http://www.jbc.org) contains supplemental Table S1.

⌘ *Author's Choice*—Final version full access.

The atomic coordinates and structure factors (code 3PCV) have been deposited in the Protein Data Bank, Research Collaboratory for Structural Bioinformatics, Rutgers University, New Brunswick, NJ (http://www.rcsb.org/).

[1] These authors contributed equally to this work.

[2] To whom correspondence may be addressed. Tel.: 81-791-58-2815; Fax: 81-791-58-2816; E-mail: ago@spring8.or.jp.

[3] To whom correspondence may be addressed. Tel.: 81-791-58-2815; Fax: 81-791-58-2816; E-mail: miyano@spring8.or.jp.

[4] The abbreviations used are: LT, leukotriene; cys-LT, cysteinyl leukotrienes; LTC_4S, LTC_4 synthase; LTA_4-Me, LTA_4 methyl ester; DDM, dodecyl-β-D-maltoside; BisTris propane, 1,3-bis[tris(hydroxymethyl)methylamino]propane; PGB_2, prostaglandin B_2; RP, reverse phase.

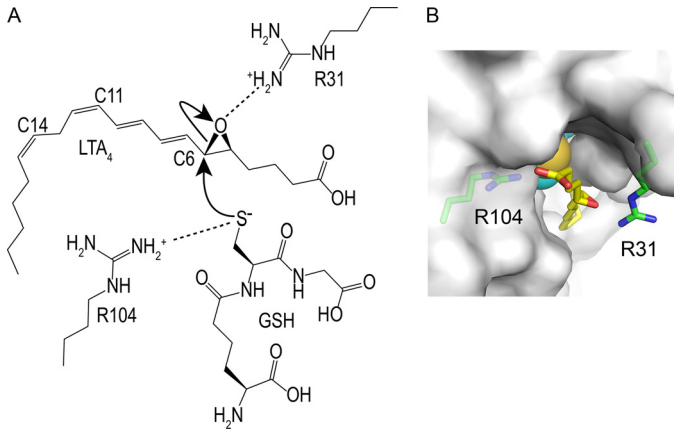

FIGURE 1. **Schematic representation of the proposed catalytic mechanism.** *A*, the catalytic mechanism for LTC_4 biosynthesis catalyzed by Arg-31 and Arg-104 was proposed from the crystal structure of LTC_4S and the putative LTA_4 binding model (35). In *panel B* the surface of the LTC_4S trimer is in *white*. The side chain of Arg-31 was flexible in the crystal structure of this work, so the side chain of Arg-31 with the most common conformation in the crystal structure is presented as a plausible model (55). The buried GSH molecule is shown by the CPK (Corey Pauling Koltun) model. The epoxide group comes to the space between the Arg-31 and Arg-104. The space is the only place where the epoxide group can interact with the thiol group, because the thiol group of GSH is buried inside of the trimer. The epoxide group can bind in a productive manner there in which the epoxy carbon comes to the proximity of the thiol group and the epoxy oxygen resides at the opposite side of the thiol group, although the binding mode of LTA_4 remains to be confirmed experimentally. The positively charged Arg-31 increases the electrophilicity of the C6 of LTA_4 by forming a hydrogen bond with the epoxide oxygen, and the positively charged Arg-31 stabilizes the negatively charged alkoxide group, which forms from the epoxide group concomitantly with the propagation of the catalysis. Through the direct interaction between the guanidino side chain of Arg-104 and the thiol group of GSH, the Arg-104 decreases the pK_a of the thiol group to the level where the thiol group becomes the activated species as a thiolate anion at physiological pH. Then, the resultant thiolate anion attacks the electrophilic C6 of LTA_4.

brane-associated proteins in eicosanoid and glutathione metabolism family. Tyr-93 and Arg-51, which had been proposed to be responsible for this catalysis based on the previous site-directed mutagenesis analysis (37), were included in the nine amino acid residues for GSH binding. Arg-104 is the only amino acid residue interacting with the thiol group and has been proposed to activate the thiol group of GSH (Fig. 1).

The details on the catalytic activity of LTC_4 biosynthesis by LTC_4S remain to be determined. Based on the previous x-ray crystal structure of the LTC_4S-GSH complex, how GSH is bound and activated was proposed. However, the amino acid residue(s) that is directly involved in the catalysis of LTA_4 was elusive without LTA_4 complex structure. We hypothesized that there is a certain amino acid residue forming a hydrogen bond with the epoxide oxygen of LTA_4, because protonation of the epoxide group of LTA_4 has a powerful impact on the reactivity of LTA_4. The epoxide group of LTA_4 is hydrolyzed readily in acidic solution, whereas it is less reactive in basic solution (38). In fact, to prepare LTA_4 from LTA_4 methyl ester (LTA_4-Me), the hydrolysis of the methyl group of LTA_4-Me proceeds without ring opening of the epoxide group in a basic solution, such as 0.25 M NaOH/acetone, as shown in the product insert from the supplier (Cayman Chemical) and the previous literature (39).

We have proposed that the Arg-31 is the amino acid residue interacting with the epoxide oxygen based on the putative LTA_4 binding model (Fig. 1) (35). LTA_4 binding models based on the binding of the hydrocarbon tail of dodecyl maltoside in the hydrophobic part of the active site have been proposed (35, 36). The proposed position of the epoxide group is a plausible position for the catalysis, although the proposed binding mode of LTA_4 is still controversial due to a lack of the structural complex for LTC_4S and LTA_4. Nevertheless, the proposed LTA_4 binding mode is consistent with the 5*S*-hydroxyl-6*R*-glutathionyl product stereochemistry by the S_N2 nucleophilic substitution, where the C6 carbon as the electrophile faces the thiol group of GSH at the narrow path and the leaving epoxy oxygen at the other side of C6. In such a case, Arg-31, the side chain reaches the epoxide group in the putative LTA_4 model, suggesting a catalytic role for Arg-31 in the reactivity of LTA_4. Arg-31 was proposed to make the epoxide group reactive by forming a hydrogen bond with the epoxide oxygen in the carrying out of the catalytic mechanism. An enzymatic assay is needed to confirm the putative functions of these arginine residues suggested by the crystal structure.

Based on the enzyme assay performed on the wild-type (WT) and mutant LTC_4S, here we report that the two arginine residues Arg-31 and Arg-104 are the catalytic amino acid residues specific for LTA_4 and GSH, respectively. The decreased k_{cat}/K_m of the mutant LTC_4S missing Arg-31 or Arg-104 showed that the arginine residues closely participate in the catalysis. A comparison of the pH dependence of k_{cat} and K_m between WT LTC_4S and these mutants showed that Arg-31 has the LTA_4 activating, but not binding function of LTA_4, and Arg-104 plays a role in both the activating and binding of GSH.

EXPERIMENTAL PROCEDURES

Site-directed Mutagenesis—Plasmids for the mutants of human LTC_4S in which alanine replaced Arg-31 (R31A) or Arg-104 (R104A), respectively, were prepared using a QuikChange mutagenesis XLII kit (Stratagene). A QuikChange lightning mutagenesis kit (Stratagene) was used for preparation of the expression plasmids in which alanine replaced Arg-90 (R90A), Arg-92 (R92A), Arg-99 (R99A), or Arg-113 (R113A) or glutamine replaced Arg-31 (R31Q), Arg-90 (R90Q), Arg-92 (R92Q), Arg-99 (R99Q), Arg-104 (R104Q), or Arg-113 (R113Q) or glutamic acid replaced Arg-31 (R31E) or leucine replaced Arg-31 (R31L). The template was the pESP-3 expression vector (Stratagene) carrying human LTC_4S with a His_6 tag at its C terminus (35, 40). The primers for the mutation works are shown in supplemental Table S1.

Protein Expression and Purification—The resultant plasmids of each mutant as well as the plasmid for WT LTC_4S were introduced into *Schizosaccharomyces pombe h⁻ leu1-32* using the lithium acetate method (41), and stable clones were established. Expression of WT and mutant LTC_4S were induced by the depletion of thiamine in the culture media, as the promoter of the plasmid is highly activated by the depletion of thiamine.

The proteins for the enzyme assay were purified as described (35) with an omission of the last PD-10 desalting step. Thus, LTC_4S was eluted from a Superose-12 column equilibrated with a solution of 20 mM MES-NaOH (pH 6.5), 0.1 M NaCl, 0.04% (w/v) dodecyl-β-D-maltoside (DDM), 1 mM DTT, 10%(v/v) glycerol, and 5 mM GSH and was concentrated to ~5

mg/ml and then stored at −80 °C. Concentrations of the purified enzymes were determined based on UV absorption at 280 nm and the milligram extinction coefficients, 1.57 $mg^{-1} \cdot cm^{-1}$. The purified samples were confirmed to be a single band using SDS-polyacrylamide gel electrophoresis.

The recombinant enzymes for the crystallographic work were additionally applied to a PD-10 column equilibrated with a solution of 20 mM MES-NaOH (pH 6.5), 0.04%(w/v) DDM, and 5 mM GSH. The recombinant enzymes eluted from the PD-10 column were concentrated to 6.0 mg/ml for WT LTC_4S, 5.4 mg/ml for the R31A mutant, and 2.9 mg/ml for the R104A mutant.

Crystallography—The crystals of WT LTC_4S and the R31A mutant were grown at 20 °C from a mother solution composed of equal amounts of the enzyme solution and the reservoir solution containing 0.1 M MES-NaOH (pH 6.5), 1.6 M ammonium sulfate, and 0.8 M magnesium chloride. The crystals of WT LTC_4S were transferred into the harvest solution of 0.1 M MES-NaOH (pH 6.5), 2.4 M ammonium sulfate, and 45 mM GSH. The crystals were dipped into the harvest solution supplemented with 15%(v/v) ethylene glycol before the x-ray diffraction experiment at a cryogenic temperature using BL26B2/SPring-8 (42). The statistical data for the diffraction data are shown in Table 1.

The crystals of the R104A mutant were grown under conditions that were virtually the same as in the previous case (35). The R104A mutant was mixed with the reservoir solution (28% (v/v) PEG400, 0.1 M MOPS-NaOH (pH 7.0)) in equal amounts and incubated at 4 °C for 2 weeks. The crystals grown were frozen at a cryogenic temperature, and diffraction images were taken with a BL44B2/SPring-8 (43).

The structural comparison between the WT LTC_4S and the mutants of R31A and R104A was performed by the difference Fourier method to assess whether the three-dimensional structure of LTC_4S suffered damage from the point mutations. The Fourier coefficients and phases were $F_{R31A(F23)} - F_{WT(F23)}$, $\phi_{WT(F23)}$ or $F_{R104A(C2221)} - F_{WT(C2221)}$, $\phi_{WT(C2221)}$, and $F_{R31A(F23)}$ and $F_{R104A(C2221)}$ are structure factors of the R31A and R104A mutant crystals with the space group F23 and $C222_1$, respectively. $F_{WT(F23)}$ is structure factor of the WT LTC_4S crystal in this work, and $\phi_{WT(F23)}$ is the phase calculated from the refined structure of WT LTC_4S. $F_{WT(C2221)}$ is structure factor of the WT LTC_4S crystal used in the previous study (PDB ID 2PNO), and $\phi_{WT(C2221)}$ is the phase calculated from the coordinate of WT LTC_4S (PDB ID 2PNO) (35). The computer programs employed were MOSFLM, SCALA, and TRUNCATE for the processing of diffraction images, AMORE and MOLREP for molecular replacement, REFMAC5 and COOT for the structural refinement (44), and PyMOL for the structural inspection and preparation of figures for structural representation.

Far Ultraviolet Circular Dichroic Analysis—Far ultraviolet circular dichroic (CD) spectra of WT LTC_4S and the R31A and R104A mutants at 4.0 °C were measured with a J-715 spectropolarimeter (Jasco). The purified enzymes were applied to a PD-10 column equilibrated with a solution of 2.5 mM MES-NaOH (pH 6.5), 0.04% (w/v) DDM.

Relative Enzyme Activities of Arginine Mutants in Comparison to the WT LTC_4S—The effects of point mutation on one of arginine residues around the entrance of GSH binding site were assessed by the determination of the relative activity of the Arg mutants in comparison with that of WT LTC_4S. The conditions for this enzyme assay were 20 ng of enzyme in 200 μl of the solution (10 mM GSH, 21.2 μM LTA_4-Me, or 20.0 μM LTA_4, 50 mM BisTris propane (pH 7.0), 10 mM $MgCl_2$, 0.015% DDM) at room temperature and an incubation time of 2 min. To terminate the enzyme reaction, 608 μl of a solvent of methanol:acetic acid (75:1 by volume) containing prostaglandin B_2 (PGB_2) as the internal standard for reverse phase HPLC (RP-HPLC) assay was added. One hundred μl of the final 808-μl solution was applied to the RP-HPLC analysis. The assays for each condition were repeated at least three times.

The LTA_4-Me purchased from Cayman Chemical was dried under N_2 stream and then solved by ethanol with 3%(v/v) triethylamine, and the ethanol solution was used for the assay. LTA_4 was prepared from LTA_4-Me by the method described in the product insert (Cayman Chemical). The concentrations of LTA_4-Me or LTA_4 were determined by UV absorbance at 280 nm (the molar extinction coefficients (ϵ) = 49,000, as shown in the product insert).

Determination of Kinetic Parameters—To determine the kinetic parameters of WT LTC_4S and the R31A and R104A mutants, the enzyme activities were measured with varying concentrations of GSH at pH 7.0, 8.0, and 9.0 at room temperature. Enzyme catalysis was started by the addition of 2 μl of LTA_4-Me (1.9–2.0 mM) to 198 μl of solution containing 50 mM BisTris propane (pH 7.0, 8.0, 9.0), 10 mM $MgCl_2$, 9.85–0.05 mM GSH for WT LTC_4S, 3.11–0.05 mM GSH for R31A, 49.1–0.05 mM GSH for R104A, 0.015% (w/v) DDM, and the enzyme. The enzyme amounts and reaction times were optimized to detect LTC_4-Me by RP-HPLC; WT, 20 ng of enzyme and 1 min reaction; R31A, 600 ng and 10 min; R104A, 200 ng and 8 min. The enzyme assay was terminated as described above.

Assays with varying concentrations of LTA_4-Me were also performed for WT LTC_4S and the R31A and R104A mutants. The reactions were initiated by a 2-μl aliquot of LTA_4-Me to 198 μl of solution of 50 mM BisTris propane (pH 7.0, 8.0, 9.0), 10 mM $MgCl_2$, 10 mM GSH, 0.015% (w/v) DDM, and an appropriate amount of enzyme (WT LTC_4S, 20 ng; R31A and R104A mutants, 600 ng). The final concentrations of LTA_4-Me were 21.2–0.5 μM for WT LTC_4S and 10.6–1.1 μM for the R31A and R104A mutants. The reaction times for WT LTC_4S and the R31A and R104A mutants were 2, 8, and 8 min, respectively. The enzyme assays was terminated as described above. The enzyme assay using LTA_4 was performed to clarify whether the terminal carboxyl group of LTA_4, which is esterified to be a methyl ester in LTA_4-Me, exerted an affect on the specificity constant.

The specificity constants (k_{cat}/K_m) of the WT LTC_4S at pH 7.0 for GSH with a fixed LTA_4 concentration (20 μM) and for LTA_4 with a fixed GSH concentration (10 mM) were measured following the method described above. The concentration of GSH was varied from 2 to 10 mM for the k_{cat}/K_m of GSH, and the concentration of LTA_4 was changed from 1 to 20 μM for the k_{cat}/K_m of LTA_4. The reaction time of this assay was 2 min.

TABLE 1
Statistics of diffraction data

WT LTC_4S

Cell dimensions	a = b = c = 168.0 Å							
Space group	F23							
Beam Line	BL26B2/SPring-8 with the newly developed dynamic sagittal-focusing monochromator.							
	Resolution (Å)		R_{merge}	Number of observations		$I/\sigma(I)$	Completeness	Multiplicity
	Low	High		Total	Unique		(%)	
Over all	19.8	1.9	0.080	305,547	30,950	4.7	99.9	9.9
Inner Shell	19.8	6.0	0.053	25,689	1,005	9.7	97.3	25.6
Outer Shell	2.0	1.9	0.302	34,698	4,517	2.4	100.0	7.7
Refinement	Resolution (Å)		19.8 - 1.90					
	R / R_{free}		0.179 / 0.198 (0.225 / 0.246)[a]					
	r.m.s. deviations							
	Bond lengths (Å)		0.013					
	Bond angles (°)		1.174					

R31A

Cell dimensions	a = b = c = 168.1 Å							
Space group	F23							
Beam Line	BL26B2/SPring-8							
	Resolution (Å)		R_{merge}	Number of observations		$I/\sigma(I)$	Completeness	Multiplicity
	Low	High		Total	Unique		(%)	
Over all	38.6	2.7	0.081	240,758	10,946	6.2	100.0	22.0
Inner Shell	38.6	8.5	0.073	6,735	371	6.8	99.2	18.2
Outer Shell	2.9	2.7	0.226	36,198	1,592	3.2	100.0	22.7

R104A

Cell dimensions	a = 117.4 Å, b = 296.2 Å, c = 207.2 Å							
Space group	$C222_1$							
Beam Line	BL44B2/SPring-8							
	Resolution (Å)		R_{merge}	Number of observations		$I/\sigma(I)$	Completeness	Multiplicity
	Low	High		Total	Unique		(%)	
Over all	23.3	4.2	0.167	191,227	26,590	4.2	99.3	7.2
Inner Shell	23.3	13.3	0.046	3,240	724	11.4	79.5	4.5
Outer Shell	4.4	4.2	0.424	28,597	3,868	1.8	100.0	7.4

[a] The numbers in the parentheses are R and R_{free} at the high resolution shell (1.95-1.90Å).

Quantification of LTC_4-Me or LTC_4 in a 100-μl aliquot of the 808-μl terminated sample was carried out by RP-HPLC, as described below. The assays for each condition were repeated at least three times. GraphPad Prizm5.0a was used for the calculation of the kinetic parameters by non-linear regression analysis with the Michaelis-Menten equation.

Reverse Phase HPLC Analysis—The quantification of LTC_4-Me was performed using RP-HPLC with a SYSTEM GOLD 126 solvent module, a 168 detector, a 508 autosampler (Beckman-Coulter) (37), and a YMC-Pack PolymerC18 (4.6- × 250-mm, S-6 μm). The column was equilibrated with solvent A at a flow rate of 1 ml/min. A mixture of 80 ml of methanol, 120 ml of acetonitrile, and 1.6 ml of acetic acid was diluted to 1 liter by water, and then the pH of the solution was adjusted to pH 6.0 by small aliquots of ethanolamine to prepare solvent A. Solvent B for the RP-HPLC analysis was 100% methanol. The mobile phase for the assay with LTA_4-Me and that for the assay with LTA_4 were 61 and 48% solvent B, respectively, and it was main-

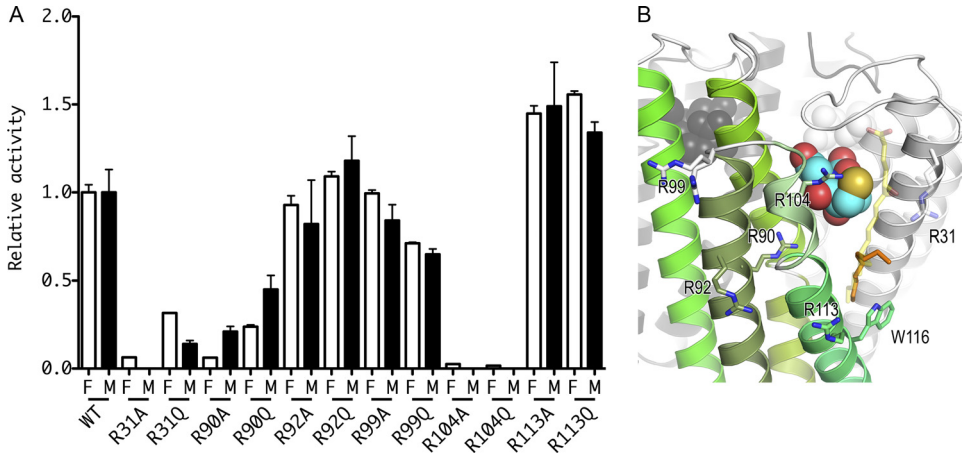

FIGURE 2. **Relative activities of the arginine mutants in comparison to WT LTC_4S.** *A*, relative activities of the arginine mutants in comparison to WT LTC_4S are shown with S.D. The enzyme activities of the mutant enzymes with LTA_4 and LTA_4-Me were normalized to the enzyme activities of the WT LTC_4S with LTA_4 and LTA_4-Me, respectively. The *open* and the *closed bars* depict the relative enzyme activities measured using LTA_4 (*F*) and LTA_4-Me (*M*), respectively. *B*, the arginine residues mutated in this work are shown by *stick models*. The ribbon model with *green* is a monomer in the LTC_4S trimer, and the other two are shown in *gray*. The *translucent stick model* with *yellow carbons* represents the putative LTA_4 binding model, and the alkyl chain of the dodecyl maltoside used for the modeling of the LTA_4 is shown by the *stick model* with *orange carbons*. The conformation of the side chain of Arg-31 is the one most commonly observed (55). The side chain did not have a uniform conformation in the crystal structure. Therefore, the side chain of Arg-31 modeled was represented by the *translucent stick model*.

tained for 13 min after injection of the sample. Then solvent B was increased to 100% without delay and maintained at this level for 7 min. Subsequently, solvent B was returned to that of the first mobile phase for each assay without delay and kept thus for 10 min. The quantification of LTC_4-Me or LTC_4 was performed based on the ratio between the integrated areas of PGB_2 as the internal standard and LTC_4-Me or LTC_4. In this quantification the molar extinction coefficients at 280 nm for LTC_4-Me or LTC_4 and for PGB_2 were 40,000 (45) and 28,000 (the product insert (Cayman Chemical)), respectively. The retention times of PGB_2 and LTC_4-Me in the mobile phase of 61% solvent B were 6.5 and 9.7 min, respectively. The retention times of PGB_2 and LTC_4 in the mobile phase of 48% solvent B were 12.4 and 9.1 min, respectively.

Statistical Analysis—Statistical analysis of the data was by one-way analysis of variance and multiple comparison test. Values of $p < 0.05$ were considered significant.

RESULTS

Relative Activities of the Arg Mutants of LTC_4S in Comparison to WT LTC_4S—The arginine residues around the entrance of the active site, *i.e.* Arg-31, Arg-90, Arg-92, Arg-99, Arg-104, and Arg-113, were each subjected to point mutations to evaluate the enzyme activity in comparison to WT LTC_4S (Fig. 2). Both LTA_4 and LTA_4-Me were used as a substrate to evaluate whether the terminal carboxyl group of LTA_4 affects the relative activity or not because the negatively charged carboxyl group of LTA_4 would interact with certain mutated arginine residue(s). Contrarily, LTA_4-Me is a neutral substrate analog with the esterified carboxyl group, resulting in more stable state in aqueous solution (46). LTA_4-Me has been used broadly as an alternate substrate instead of LTA_4 (37, 47).

The enzyme activity of the mutants of R31A, R90A, R104A, and R104Q was significantly decreased as compared with that of WT LTC_4S ($p < 0.001$). The relative enzyme activities of R31A, R90A, R104A, and R104Q for LTA_4 were 0.06 ± 0.002, 0.06 ± 0.001, 0.02 ± 0.006, and 0.02 ± 0.001, respectively. The relative enzyme activity of R90A for LTA_4-Me was 0.21 ± 0.03. The enzyme activities of R31A, R104A, and R104Q for LTA_4-Me were lower than the detection limit of the RP-HPLC, therefore, the relative enzyme activities were shown by 0.0 in Fig. 2*A*. Arg-31 and Arg-104 are the amino acid residues proposed to be the catalytic amino acid residues in a previous report (35, 36). Arg-90 forms a hydrogen bond with the side chain of Asn-57, which is one of the nine amino acid residues that directly binds to GSH (35). Thus, Arg-90 mutations may affect the GSH binding indirectly. Further studies will be needed to elucidate the role of R90 in the catalysis.

We further assessed the enzyme activities of mutant enzymes in which Arg-31 was replaced by a glutamic acid residue (R31E) or a leucine residue (R31L), because R31Q exhibited substantial activity even though the enzyme activity of the R31Q mutant was reduced significantly compared with WT LTC_4S ($p < 0.001$). The relative enzyme activities of R31Q, R31E, and R31L using LTA_4 as the substrate were 0.32 ± 0.003, 0.03 ± 0.001, and 0.03 ± 0.001, respectively, and all of these results are statistically significant in comparison to WT LTC_4S ($p < 0.001$).

The enzyme activities of all of the Arg-104 mutants were obviously decreased. The mutants of Arg-31, the side chain of which is hydrophobic or negatively charged, exhibited reduced enzyme activities, whereas R31Q, the side chain of which is a neutral hydrophilic one, maintained substantial enzyme activity. The suppression effect of R31 mutations was profound for both LTA_4 and LTA_4-Me, although the effect for LTA_4 was slightly more modest. Thus, the modification of the terminal carboxyl group of LTA_4 may have some effect; however, overall the enzyme activities were substantially reduced particularly for R31 mutants.

Enzyme Kinetics Analysis of WT LTC_4S, R31A, and R104A Mutants—Because the R31A and R104A mutants displayed the most marked decrease in enzyme activity, we further assessed

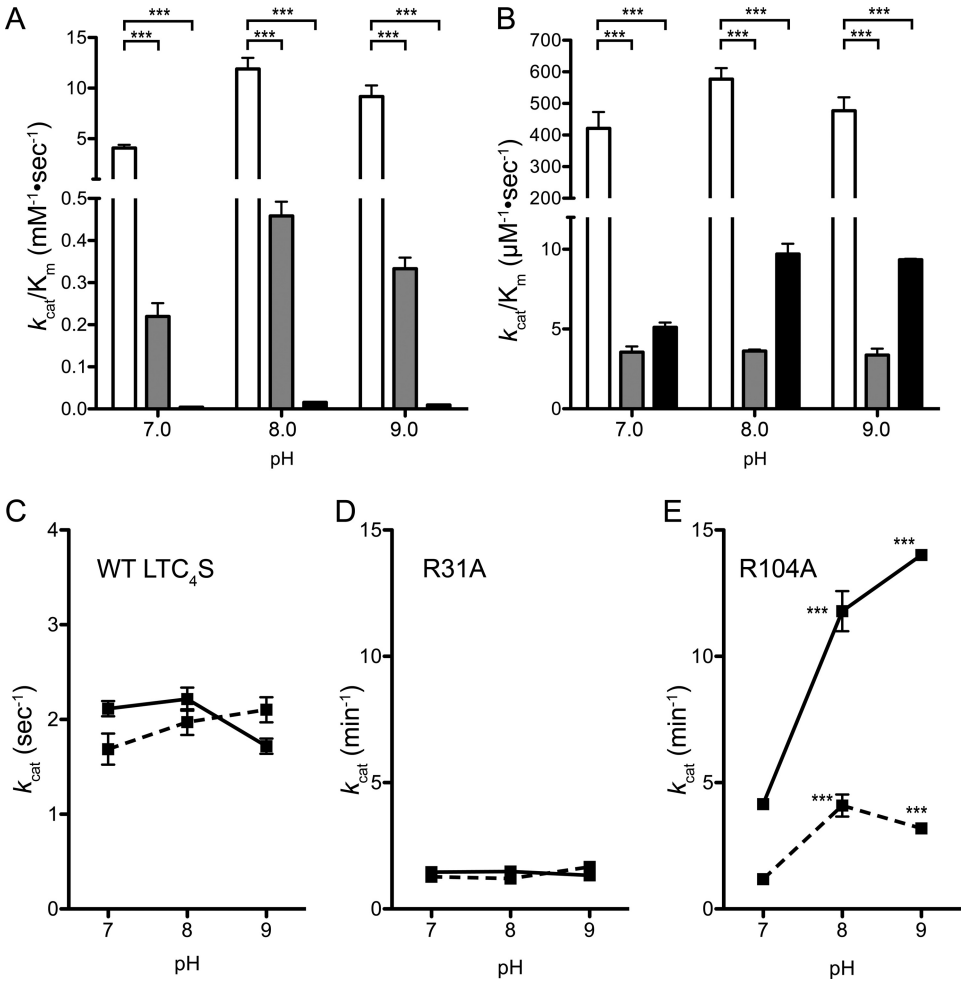

FIGURE 3. **Enzyme kinetic analysis.** In *panels A* and *B*, the k_{cat}/K_m for GSH and LTA_4-Me are, respectively, shown. The k_{cat}/K_m of WT LTC_4S and the R31A and R104A mutants are shown by the *white*, *gray*, and *black bars* with the S.D., respectively ($n = 3$). ***, $p < 0.001$. The k_{cat} with S.D. ($n = 3$) of WT LTC_4S and the R31A and R104A mutants are shown in *panels C*, *D*, and *E*, respectively. The k_{cat} values measured with the varying concentrations of GSH and LTA_4-Me are shown by the *solid* and *dashed lines*, respectively.

their enzymatic kinetic parameters. The k_{cat}/K_m of WT LTC_4S determined under varying GSH or LTA_4-Me concentrations were significantly higher than those of the R31A and R104A mutants ($p < 0.001$) (Fig. 3, *A* and *B*). All of the enzymes exhibited a higher k_{cat}/K_m at pH 8.0 than at pH 7.0 or 9.0. The k_{cat}/K_m for GSH of WT LTC_4S at pH 8.0 was 11.90 ± 1.10 mM^{-1}•s^{-1}, and it was 26- and 770-fold greater than those of the R31A (0.46 ± 0.03 mM^{-1}•s^{-1}) and R104A (0.93 ± 0.06 mM^{-1}•min^{-1}) mutants, respectively. The k_{cat}/K_m for LTA_4-Me of WT LTC_4S at pH 8.0 was 577 ± 35 μM^{-1}• s^{-1}, and it was 160-fold and 60-fold that of the R31A (3.63 ± 0.09 μM^{-1}•s^{-1}) and R104A (9.70 ± 0.64 μM^{-1}•s^{-1}) mutants, respectively.

The k_{cat}/K_m of WT LTC_4S activity for LTA_4 or LTA_4-Me as well as GSH at pH 7.0 were measured to examine the kinetic effect of the carboxyl esterification of LTA_4. The k_{cat}/K_m for LTA_4 and LTA_4-Me of WT LTC_4S at pH 7.0 were 629 ± 6 and 421 ± 52 μM^{-1}•s^{-1}, respectively. The k_{cat}/K_m for GSH of WT LTC_4S using a fixed concentration of LTA_4 and LTA_4-Me at pH 7.0 were 2.8 ± 0.1 and 4.1 ± 0.3 mM^{-1}•s^{-1}, respectively. The measured k_{cat}/K_m of WT LTC_4S with LTA_4 and LTA_4-Me were comparable.

Only the R104A mutant exhibited a significant increase of the catalytic constant (k_{cat}) between pH 7.0 and 8.0 ($p < 0.001$) (Fig. 3*E*). The k_{cat} of R104A increased from 4.15 ± 0.80 min^{-1} at pH 7.0 to 14.01 ± 0.18 min^{-1} at pH 9.0 and 11.79 ± 0.80 min^{-1} at pH 8.0 with the various GSH concentrations (the *solid line* in Fig. 3*E*) and from 1.18 ± 0.05 min^{-1} at pH 7.0 to 4.09 ± 0.44 min^{-1} at pH 8.0, then 3.19 ± 0.04 min^{-1} at pH 9.0 with the variable LTA_4-Me concentration (the *dashed line* in Fig. 3*E*). WT LTC_4S maintained a higher level of k_{cat} over the pH range measured; 1.69 ± 0.16 s^{-1} at pH 7.0, 1.97 ± 0.14 s^{-1} at pH 8.0 and 2.10 ± 0.13 s^{-1} at pH 9.0 for the varied LTA_4-Me (the *dashed line* in Fig. 3*C*), 2.11 ± 0.08 s^{-1} at pH 7.0, 2.22 ± 0.12 s^{-1} at pH 8.0, and 1.72 ± 0.08 s^{-1} at pH 9.0 for the varied GSH with a fixed LTA_4-Me concentration (the *solid line* in Fig. 3*C*). The R31A mutant maintained a k_{cat} from pH 7.0 to 9.0; the k_{cat} from the various GSH concentrations with a fixed LTA_4-Me concentration were 1.46 ± 0.02 min^{-1} at pH 7.0, 1.48 ± 0.04 min^{-1} at pH 8.0, and 1.33 ± 0.04 min^{-1} at pH 9.0 (the *solid line* in Fig. 3*D*); those from the various LTA_4-Me concentrations were 1.28 ± 0.21 min^{-1} at pH 7.0, 1.21 ± 0.11 min^{-1} at pH 8.0, and 1.66 ± 0.14 min^{-1} at pH 9.0 (the *dashed line* in Fig. 3*D*).

The R104A mutant had a Michaelis constant (K_m) for GSH higher than 10 mM over the pH range measured, in contrast to WT LTC_4S and the R31A mutant, with the K_m for GSH at the submillimolar level (Table 2). There is a difference in the pH

TABLE 2
Michaelis constants for GSH or LTA_4-Me
Values are the mean ± S.D.

	Wild type			R31A			R104A		
	pH 7.0	pH 8.0	pH 9.0	pH 7.0	pH 8.0	pH 9.0	pH 7.0	pH 8.0	pH 9.0
K_m^{GSH} mM	0.520 ± 0.032	0.188 ± 0.027[a]	0.189 ± 0.017[a]	0.104 ± 0.004	0.0541 ± 0.0053[a]	0.0669 ± 0.0078[a]	16.7 ± 0.3	12.8 ± 1.6[c]	24.6 ± 1.2[a]
$K_m^{LTA4\text{-}Me}$ μM	4.08 ± 0.90	3.44 ± 0.43	4.45 ± 0.65	6.09 ± 1.62	5.55 ± 0.62	8.39 ± 1.84	3.85 ± 0.38	7.09 ± 1.18[c]	5.69 ± 0.05[b]

[a] $p < 0.001$ as compared to pH 7.0.
[b] $p < 0.05$ as compared to pH 7.0.
[c] $p < 0.01$ as compared to pH 7.0.

dependence of K_m for GSH between the enzymes with and without Arg-104. The K_m for GSH of the WT LTC_4S at pH 7.0 was significantly higher than at pH 8.0 or 9.0. The pH dependence of the K_m for the GSH of WT LTC_4S is comparable with that of the R31A mutant but not the R104A mutant. The R104A mutant had a higher K_m for GSH at pH 9.0 than pH 7.0. All enzymes, including the R104A mutant, had a comparable K_m for LTA_4-Me, although only the R104A mutant exhibited a pH-dependence of K_m for LTA_4-Me.

Structural Verification of the R31A and R104A Mutants—To elucidate the role of an individual amino acid residue, it is essential that the mutant enzyme does not suffer damage from the point mutation. Using the crystallographically isomorphous crystals of a mutant enzyme and the WT LTC_4S, the difference Fourier method makes it possible to clarify whether there are any differences between the structures of a given mutant enzyme and the WT LTC_4S.

We obtained crystallographically isomorphous crystals of the R31A mutant and the WT LTC_4S with the space group F23 and a crystal of the R104A mutant isomorphous with the crystal of WT LTC_4S with the space group $C222_1$, as described previously (35). The crystallographic parameters and the statistics of the diffraction data from those crystals are shown in Table 1.

The crystal structure of WT LTC_4S at 1.9 Å resolution with the space group F23 was refined successfully. The crystallographic R and R_{free} values were 0.179 and 0.198 for the diffraction data and 0.225 and 0.246 for the highest resolution shell of 1.95 to 1.90 Å, respectively (Table 1). There was no amino acid residue with the disallowed main chain dihedral angle of ϕ or ψ on the Ramachandran plot.

The overall structure of LTC_4S presented here is basically identical to those previously reported (Fig. 4) (35, 36). In a superimposition between the current and previous structures, the root mean square deviations of the corresponding Cα atoms, except for those from the fifth α-helix extruding into the bulk solvent, are less than 0.4 Å. The architecture for GSH binding is conserved (Fig. 4*B*). The GSH binding site is a V-shaped cleft at each intermonomer interface in the LTC_4S trimer, and nine amino acid residues directly participate in the GSH binding. The minor differences between the current and previous structures are the side-chain conformations of Arg-30 and Arg-104. In the current structure, as shown by the model with the *green carbons* in Fig. 4*B*, Arg-30 multiply binds the carboxyl group of the γ-glutamyl moiety, and Arg-104 interacts with both the thiol group and the carbonyl group of the cysteinyl moiety of GSH. The current side chain conformations of Arg-30 and Arg-104 are similar to those observed in the crystal grown with ammonium sulfate rather than polyethylene glycol

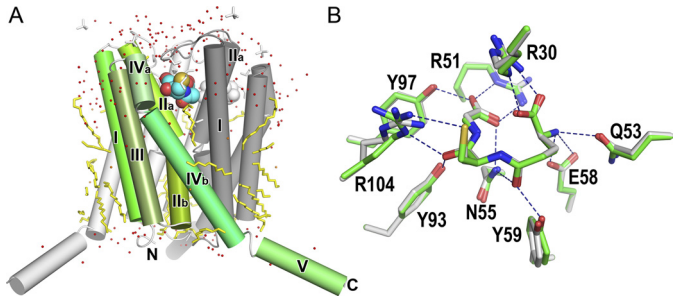

FIGURE 4. **Crystal structure of WT LTC_4S at 1.9 Å resolution.** *A*, the crystal structure of LTC_4S was determined to be a trimer with a three-fold axis at the center. Each monomer in the LTC_4S trimer is colored *green* with gradations, *light gray*, and *dark gray*. The *roman numeral* shows the sequential order of the α-helix from the N-terminal. *Stick models in yellow* show the hydrocarbon tails of the dodecyl maltosides. The *stick models in white* are ethylene glycols or sulfate ions. The Corey-Pauling-Koltun model represents the bound GSHs. The characters *N* and *C* indicate the N and C termini of the current model. *B*, superimposition of the GSH binding sites is shown. The GSH binding sites of the current study (*green carbons*; this work) and previous studies (*white carbons*; PDB ID 2PNO) are superimposed. *Dashed lines* show the polar intermolecular interactions of less than 3.5 Å.

as the precipitant agent (35, 36). The side chain of Arg-31 was flexible in the crystal structure, and the electron density corresponding to the side chain before the Cβ of Arg-31 was not apparent in the electron density map contoured at 1.2σ. This refined crystal structure of WT LTC_4S allowed us to visualize the structural differences between WT LTC_4S and the mutants of R31A by the difference Fourier method.

The R104A mutant was crystallized using the conditions as previously reported (35). Under the current crystallization conditions with ammonium sulfate and magnesium chloride as the precipitant agents, WT LTC_4S, in which the guanidino side chain of Arg-104 binds a sulfate ion, crystallized in the space group F23, but the R104A mutant missing the side chain of Arg-104 did not crystallize. Thus, we used the previous crystallization conditions with polyethylene glycol 400 as the precipitant agent for crystallization of the R104A mutant. The R104A mutant crystallized in the space group $C222_1$.

There were no significant residual electron densities, except for the residual electron density corresponding to the side chain of the mutated amino acid residue in both of the difference Fourier electron density maps for each pair of the isomorphous crystals (Fig. 5). The difference Fourier electron density maps supported the conclusion that the three-dimensional structures of the R31A and R104A mutants did not suffer any damage from the point mutations.

The far-ultraviolet CD analysis showed that the secondary structure composition of WT LTC_4S and the R31A and R104A mutants in solution were not distinguishable from each other. The percentages of the secondary structure of WT LTC_4S,

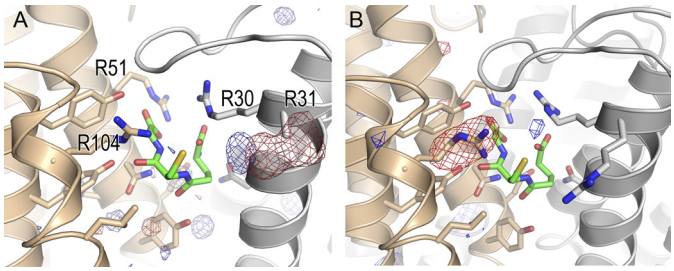

FIGURE 5. **Difference Fourier maps of the R31A and R104A mutants.** The difference Fourier electron density maps for R31A (*panel A*) and R104A (*panel B*) were calculated from Fourier coefficients and the phases of $F_{R31A(F23)} - F_{WT(F23)}$, $\phi_{wt(F23)}$ and $F_{R104A(C2221)} - F_{WT(C2221)}$, $\phi_{wt(C2221)}$, respectively. The *R*-factors between the diffraction intensity data of the WT LTC_4S and the R31A mutant and between the diffraction intensity data of the WT LTC_4S and the R104A mutant were 0.082 and 0.192, respectively. The map for R31A was contoured at $+4.5\sigma$ (*blue*) and -4.5σ (*red*), and that for R104A was contoured at $+4\sigma$ (*blue*) and -4σ (*red*). The atomic models in *panel A* and *B* are the WT LTC_4S in this work and the previous work (PDB ID 2PNO), respectively.

R31A, and R104A estimated from each CD spectrum were similar to each other; the percentages of the α-helix, β-strand, and random loop of WT LTC_4S were 69, 4, and 27%, respectively, whereas those of R31A were 64, 6, and 30%, and those of R104A were 62, 6, and 32%. The percentages were calculated by the K2d program (48). Thus, both the x-ray crystallographic analysis and the CD analysis of the WT LTC_4S, R31A, and R104A mutants confirmed that there was no significant structural difference between their three-dimensional structures.

DISCUSSION

Based on the previous x-ray crystallographic studies, we proposed that Arg-31 and Arg-104 constitute the catalytic architecture for conjugating LTA_4 and GSH in the active site of LTC_4S (Fig. 1) (35). To investigate further, we prepared mutant enzymes and performed the assays for enzymatic analysis to obtain first order kinetics as well as verification of the three-dimensional structures of the mutants.

Role of Arg-31 and Arg-104 in the Catalysis—The k_{cat}/K_m of the WT LTC_4S measured at pH 7.0, 8.0, and 9.0 were significantly higher than both of the R31A and R104A mutants (Fig. 3, *A* and *B*). The effects of each point mutation on the three-dimensional structures of the mutants were examined by the crystallographic and CD analyses. Using each corresponding isomorphous crystal, there were no indications of any significant structural changes in the difference Fourier maps between each mutant and the WT LTC_4S other than the mutated residue, Arg-31 or Arg-104 (Fig. 5). In the CD analyses, the secondary structural elements of these mutants were similar to those of WT LTC_4S. These results support the conclusion that the decreased k_{cat}/K_m of the mutants in comparison with WT LTC_4S was caused by the lack of the side chain of Arg-31 or Arg-104, not by denaturing or partial unfolding imposed by the point mutation. It cannot be excluded that a certain minor structural perturbation may occur that is undetectable by the CD and the crystallographic analyses. As discussed below, Arg-31 and Arg-104 may play distinct roles in the enzymatic catalysis and cooperate to propagate conjugation between GSH and LTA_4 at physiological pH levels.

The binding function of Arg-104 for GSH was established because the R104A mutant exhibited a higher K_m for GSH than the WT LTC_4S and R31A mutants, in which the K_m values are at the submillimolar level (Table 2). Furthermore, the pH dependence of the K_m for the GSH of the WT LTC_4S, R31A, and R104A mutants supports the binding function of Arg-104, as discussed below. The K_m for the GSH of the WT LTC_4S and R31A mutant was significantly decreased at pH 8.0 and higher pH ($p < 0.001$ against pH 7.0). The K_m for the GSH of the R104A mutant increases at pH9.0 ($p < 0.001$), with a decrease at pH 8.0 ($p < 0.05$), in comparison with that at pH 7.0. The decreased K_m for GSH at alkaline pH indicates that the enzymes with Arg-104 retained a higher affinity for GSH at the alkaline pH measured, in contrast to that of the enzyme without Arg-104, having a lower affinity for GSH at pH 9.0. The positively charged guanidino side chain of Arg-104 interacts with the thiol group of GSH directly in the crystal structure. The thiol group of GSH becomes a negatively charged thiolate anion at alkaline pH. Thus, attractive interaction between the positively charged side chain of Arg-104 and the negatively charged thiolate anion of GSH at alkaline pH contributes to the maintenance of the high affinity for GSH at alkaline pH.

In addition to the binding function, the pH-dependent increase of the k_{cat} of the R104A mutant to approximately the pK_a of the thiol group shows the GSH activating function of Arg-104 at physiological pH (Fig. 3). The value of k_{cat} is correlated to deprotonation of the thiol group, resulting in the formation of the thiolate anion as the active species in the catalysis. WT LTC_4S has k_{cat} values which are just as high at pH 7.0 as at a pH of 8.0 or higher. Therefore, the thiol group in the active site of WT LTC_4S is considered to be deprotonated, even at pH 7.0. In contrast, the k_{cat} of the R104A mutant increases in a pH-dependent manner. The k_{cat} of the R104A mutant at pH 8.0 and pH 9.0 is ~3-fold higher than at pH 7.0. Thus, the thiolate anion in the active site missing the Arg-104 increases at pH values higher than pH 7.0. The pH dependence profile of the deprotonation of GSH in the active site of the R104A mutant is concluded to be similar to that of free GSH with a normal pK_a (49). Thus, the guanidino side chain interacting with the thiol group of GSH is responsible for the activation of the thiol group at pH 7.0 as well as the binding function of GSH, as discussed above.

We have proposed that the guanidino side chain of Arg-31 forms a hydrogen bond with the epoxide oxygen, resulting in the formation of an electron deficient epoxide carbon as the target of nucleophilic attack by the thiolate anion of GSH at the initiation of catalysis (Fig. 1) (35). This is because the protonation of the epoxide group of LTA_4 has a significant impact on the reactivity of the epoxide group (38, 39). Although the guanidino side chain of arginine has an extremely high pK_a, the guanidino side chain can form a hydrogen bond with various polar functional groups, such as hydroxyl groups so forth (50, 51). Furthermore, recent computational studies have proposed that the guanidino side chain of arginine residue can act as a general acid (52, 53). We have also proposed that Arg-31 neutralizes a negative charge growing on the epoxide oxygen in the propagation of the nucleophilic attack on the electro-deficient carbon by the thiol group of GSH (Fig. 1) (35).

The enzymatic assay results for the R31A mutant were consistent with the previous proposal for the roles of Arg-31 in the catalysis (35). The remarkably decreased k_{cat} and k_{cat}/K_m value

of the R31A mutant in comparison to that of the WT LTC_4S suggested that the side chain of Arg-31 interacts with a catalytically essential functional group of LTA_4-Me (Fig. 3). The pH dependence of k_{cat} of the R31A mutant, which was similar with that of the WT-LTC_4S, showed that the side chain of Arg-31 may interact with the functional group of LTA_4-Me, having a pK_a outside of the measured pH range. The epoxide group of LTA_4 is the essential functional group and also has a pK_a outside of the measured pH range. This supports Arg-31 being the amino acid residue that interacts with the epoxide group of LTA_4.

Arg-31, but not bulk water, is supposed to form an effective hydrogen bond with the epoxide oxygen, accelerating the enzymatic catalysis. The R31A mutant with Ala-31, having a small apolar side chain, the R31L mutant with Leu-31, with a large apolar side chain, and the R31E mutant with Glu-31, having a negatively charged polar side chain, instead of Arg-31, with the longest and positively charged polar guanidino side chain, exhibited enzyme activity reduced to less than one tenth of the WT LTC_4S (Fig. 2*A*). In contrast, the R31Q mutant, exhibiting 30% enzyme activity in comparison to WT LTC_4S, shows that the neutral polar side chain of Gln-31 partly compensated for the role of the positively charged guanidino side chain of Arg-31 (Fig. 2*A*). Gln-31 cannot interact directly with an epoxide group such as Arg-31 due to the side chain being shorter than that of the arginine residue; thus, Gln-31 might affect the epoxide group through the hydrated water molecule(s) of the polar side chain of Gln-31. In addition, the drastically decreased enzymatic activity of the R31A and R31L mutants shows that the bulk water molecules are unable to compensate for the role of Arg-31 on the epoxy group. Furthermore, the R31E mutant with decreased enzyme activity shows that the negatively charged side chain of Glu-31 cannot compensate for the role of Arg-31 with the positively charged side chain, in contrast to Gln-31. The negatively charged side chain of Glu-31 makes the hydrated water molecules electrostatically negative. Therefore, the electrostatically negative water molecule hardly interacts with the negatively polarized epoxide oxygen or the negatively charged alkoxide group formed in the course of the catalysis. A polar functional group with fewer degrees of freedom of motion around the epoxide group of LTA_4, such as the guanidino side chain of Arg-31 or the hydrated water molecule of Gln-31, makes an effective hydrogen bond with the epoxide group so as to accelerate the nucleophilic attack. Arg-31 probably fits as a catalytic amino acid residue for LTA_4.

In comparison with WT LTC_4S, the R31A mutant sustained a comparable K_m for LTA_4-Me despite a much lower k_{cat} (Table 2 and Fig. 3*D*). This suggests that Arg-31 does not contribute to the LTA_4-Me binding, in contrast to the binding activity of Arg-104 for GSH.

LTC_4S has certain unique features as a nuclear membrane-embedded enzyme responsible for LTC_4 biosynthesis. In our proposed catalytic mechanism, Arg-31 and Arg-104 function as the catalytic amino acid residues by forming a hydrogen bond with LTA_4 and GSH, respectively. Arg-104 forming hydrogen bonds with the thiol group of GSH facilitates the formation of the thiolate anion as the nucleophile, and the thiolate anion attacks the epoxide carbon of LTA_4. Furthermore, Arg-104 also substantially contributes to GSH binding. Arg-31, which increases the electrophilicity of the epoxide carbon of LTA_4 through a hydrogen bond with the epoxide oxygen, makes the nucleophilic attack easy at the initial step. Concomitantly with the development of the nucleophilic attack, the protonated guanidino side chain of Arg-31 neutralizes the negative charge growing on the epoxide oxygen through the hydrogen bond. At the final step of the nucleophilic attack, Arg-31 may donate a proton at the generated alkoxide from the epoxide oxygen to transform the alkoxide group to the hydroxyl group of the product, LTC_4, because alkoxide, the pK_a of which is 16–18, is more basic than the guanidino side chain of the arginine residue (54).

The results of the enzyme assay on the mutants of Arg-31 are consistent with the current LTA_4 binding model but not sufficient to conclude that the model is correct. The model is speculated based on the crystal structure of the LTC_4S complex with the hydrocarbon tail of dodecyl maltoside at the putative LTA_4 binding site. Determination of the complexed structure of LTC_4S with LTA_4 is required to understand the LTA_4 binding mode and functional role of Arg-31; however, the crystal structure analysis of LTC_4S complexed with LTA_4 is a great challenge because LTA_4 is not stable.

Acknowledgments—We thank Shunji Goto at SPring-8/JASRI for providing the opportunity to collect the diffraction data set with the beamline optics of the newly developed dynamic sagittal-focusing monochromator.

REFERENCES

1. Rouzer, C. A., Scott, W. A., Cohn, Z. A., Blackburn, P., and Manning, J. M. (1980) *Proc. Natl. Acad. Sci. U.S.A.* **77,** 4928–4932
2. MacGlashan, D. W., Jr., Peters, S. P., Warner, J., and Lichtenstein, L. M. (1986) *J. Immunol.* **136,** 2231–2239
3. MacGlashan, D. W., Jr., Schleimer, R. P., Peters, S. P., Schulman, E. S., Adams, G. K., 3rd, Newball, H. H., and Lichtenstein, L. M. (1982) *J. Clin. Invest.* **70,** 747–751
4. Weller, P. F., Lee, C. W., Foster, D. W., Corey, E. J., Austen, K. F., and Lewis, R. A. (1983) *Proc. Natl. Acad. Sci. U.S.A.* **80,** 7626–7630
5. Barrett, N. A., Maekawa, A., Rahman, O. M., Austen, K. F., and Kanaoka, Y. (2009) *J. Immunol.* **182,** 1119–1128
6. Dahlén, S. E., Hedqvist, P., Hammarström, S., and Samuelsson, B. (1980) *Nature* **288,** 484–486
7. Weiss, J. W., Drazen, J. M., Coles, N., McFadden, E. R., Jr., Weller, P. F., Corey, E. J., Lewis, R. A., and Austen, K. F. (1982) *Science* **216,** 196–198
8. Dahlén, S. E., Björk, J., Hedqvist, P., Arfors, K. E., Hammarström, S., Lindgren, J. Å., and Samuelsson, B. (1981) *Proc. Natl. Acad. Sci. U.S.A.* **78,** 3887–3891
9. Soter, N. A., Lewis, R. A., Corey, E. J., and Austen, K. F. (1983) *J. Invest. Dermatol.* **80,** 115–119
10. Wardlaw, A. J., Hay, H., Cromwell, O., Collins, J. V., and Kay, A. B. (1989) *J. Allergy Clin. Immunol.* **84,** 19–26
11. Smith, C. M., Christie, P. E., Hawksworth, R. J., Thien, F., and Lee, T. H. (1991) *Am. Rev. Respir. Dis.* **144,** 1411–1413
12. Israel, E., Dermarkarian, R., Rosenberg, M., Sperling, R., Taylor, G., Rubin, P., and Drazen, J. M. (1990) *N. Engl. J. Med.* **323,** 1740–1744
13. Manning, P. J., Watson, R. M., Margolskee, D. J., Williams, V. C., Schwartz, J. I., and O'Byrne, P. M. (1990) *N. Engl. J. Med.* **323,** 1736–1739
14. Knapp, H. R. (1990) *N. Engl. J. Med.* **323,** 1745–1748
15. Donnelly, A. L., Glass, M., Minkwitz, M. C., and Casale, T. B. (1995) *Am. J. Respir. Crit. Care Med.* **151,** 1734–1739
16. Pacor, M. L., Di Lorenzo, G., and Corrocher, R. (2001) *Clin. Exp. Allergy* **31,** 1607–1614

17. Clark, J. D., Milona, N., and Knopf, J. L. (1990) *Proc. Natl. Acad. Sci. U.S.A.* **87,** 7708–7712
18. Rouzer, C. A. F., and Samuelsson, B. (1985) *Proc. Natl. Acad. Sci. U.S.A.* **82,** 6040–6044
19. Dixon, R. A., Diehl, R. E., Opas, E., Rands, E., Vickers, P. J., Evans, J. F., Gillard, J. W., and Miller, D. K. (1990) *Nature* **343,** 282–284
20. Woods, J. W., Evans, J. F., Ethier, D., Scott, S., Vickers, P. J., Hearn, L., Heibein, J. A., Charleson, S., and Singer, I. I. (1993) *J. Exp. Med.* **178,** 1935–1946
21. Yoshimoto, T., Soberman, R. J., Spur, B., and Austen, K. F. (1988) *J. Clin. Invest.* **81,** 866–871
22. Jakobsson, P. J., Morgenstern, R., Mancini, J., Ford-Hutchinson, A., and Persson, B. (1999) *Protein Sci.* **8,** 689–692
23. Bresell, A., Weinander, R., Lundqvist, G., Raza, H., Shimoji, M., Sun, T. H., Balk, L., Wiklund, R., Eriksson, J., Jansson, C., Persson, B., Jakobsson, P. J., and Morgenstern, R. (2005) *FEBS J.* **272,** 1688–1703
24. Shi, Z. Z., Han, B., Habib, G. M., Matzuk, M. M., and Lieberman, M. W. (2001) *Mol. Cell. Biol.* **21,** 5389–5395
25. Habib, G. M., Shi, Z. Z., Cuevas, A. A., and Lieberman, M. W. (2003) *FASEB J.* **17,** 1313–1315
26. Krilis, S., Lewis, R. A., Corey, E. J., and Austen, K. F. (1983) *J. Clin. Invest.* **71,** 909–915
27. Sala, A., Voelkel, N., Maclouf, J., and Murphy, R. C. (1990) *J. Biol. Chem.* **265,** 21771–21778
28. Lynch, K. R., O'Neill, G. P., Liu, Q., Im, D. S., Sawyer, N., Metters, K. M., Coulombe, N., Abramovitz, M., Figueroa, D. J., Zeng, Z., Connolly, B. M., Bai, C., Austin, C. P., Chateauneuf, A., Stocco, R., Greig, G. M., Kargman, S., Hooks, S. B., Hosfield, E., Williams, D. L., Jr., Ford-Hutchinson, A. W., Caskey, C. T., and Evans, J. F. (1999) *Nature* **399,** 789–793
29. Heise, C. E., O'Dowd, B. F., Figueroa, D. J., Sawyer, N., Nguyen, T., Im, D. S., Stocco, R., Bellefeuille, J. N., Abramovitz, M., Cheng, R., Williams, D. L., Jr., Zeng, Z., Liu, Q., Ma, L., Clements, M. K., Coulombe, N., Liu, Y., Austin, C. P., George, S. R., O'Neill, G. P., Metters, K. M., Lynch, K. R., and Evans, J. F. (2000) *J. Biol. Chem.* **275,** 30531–30536
30. Kim, D. C., Hsu, F. I., Barrett, N. A., Friend, D. S., Grenningloh, R., Ho, I. C., Al-Garawi, A., Lora, J. M., Lam, B. K., Austen, K. F., and Kanaoka, Y. (2006) *J. Immunol.* **176,** 4440–4448
31. Beller, T. C., Friend, D. S., Maekawa, A., Lam, B. K., Austen, K. F., and Kanaoka, Y. (2004) *Proc. Natl. Acad. Sci. U.S.A.* **101,** 3047–3052
32. Paruchuri, S., Tashimo, H., Feng, C., Maekawa, A., Xing, W., Jiang, Y., Kanaoka, Y., Conley, P., and Boyce, J. A. (2009) *J. Exp. Med.* **206,** 2543–2555
33. Paruchuri, S., Jiang, Y., Feng, C., Francis, S. A., Plutzky, J., and Boyce, J. A. (2008) *J. Biol. Chem.* **283,** 16477–16487
34. Maekawa, A., Kanaoka, Y., Xing, W., and Austen, K. F. (2008) *Proc. Natl. Acad. Sci. U.S.A.* **105,** 16695–16700
35. Ago, H., Kanaoka, Y., Irikura, D., Lam, B. K., Shimamura, T., Austen, K. F., and Miyano, M. (2007) *Nature* **448,** 609–612
36. Martinez Molina, D., Wetterholm, A., Kohl, A., McCarthy, A. A., Niegowski, D., Ohlson, E., Hammarberg, T., Eshaghi, S., Haeggström, J. Z., and Nordlund, P. (2007) *Nature* **448,** 613–616
37. Lam, B. K., Penrose, J. F., Xu, K., Baldasaro, M. H., and Austen, K. F. (1997) *J. Biol. Chem.* **272,** 13923–13928
38. Rådmark, O., Malmsten, C., Samuelsson, B., Goto, G., Marfat, A., and Corey, E. J. (1980) *J. Biol. Chem.* **255,** 11828–11831
39. Carrier, D. J., Bogri, T., Cosentino, G. P., Guse, I., Rakhit, S., and Singh, K. (1988) *Prostaglandins Leukot. Essent. Fatty Acids* **34,** 27–30
40. Schmidt-Krey, I., Kanaoka, Y., Mills, D. J., Irikura, D., Haase, W., Lam, B. K., Austen, K. F., and Kühlbrandt, W. (2004) *Structure* **12,** 2009–2014
41. Okazaki, K., Okazaki, N., Kume, K., Jinno, S., Tanaka, K., and Okayama, H. (1990) *Nucleic Acids Res.* **18,** 6485–6489
42. Ueno, G., Kanda, H., Hirose, R., Ida, K., Kumasaka, T., and Yamamoto, M. (2006) *J. Struct. Funct. Genomics* **7,** 15–22
43. Adachi, S., Oguchi, T., Tanida, H., Park, S. Y., Shimizu, H., Miyatake, H., Kamiya, N., Shiro, Y., Inoue, Y., Ueki, T., and Iizuka, T. (2001) *Nucl. Instrum. Methods Phys. Res. A* **467,** 711–714
44. Collaborative Computational Project Number 4 (1994) *Acta Crystallogr. D Biol. Crystallogr.* **50,** 760–763
45. Lewis, R. A., Austen, K. F., Drazen, J. M., Clark, D. A., Marfat, A., and Corey, E. J. (1980) *Proc. Natl. Acad. Sci. U.S.A.* **77,** 3710–3714
46. Maycock, A. L., Anderson, M. S., DeSousa, D. M., and Kuehl, F. A., Jr. (1982) *J. Biol. Chem.* **257,** 13911–13914
47. Lam, B. K., Penrose, J. F., Freeman, G. J., and Austen, K. F. (1994) *Proc. Natl. Acad. Sci. U.S.A.* **91,** 7663–7667
48. Andrade, M. A., Chacón, P., Merelo, J. J., and Morán, F. (1993) *Protein Eng.* **6,** 383–390
49. Chen, W. J., Graminski, G. F., and Armstrong, R. N. (1988) *Biochemistry* **27,** 647–654
50. Gu, Y., Singh, S. V., and Ji, X. (2000) *Biochemistry* **39,** 12552–12557
51. Hoff, R. H., Hengge, A. C., Wu, L., Keng, Y. F., and Zhang, Z. Y. (2000) *Biochemistry* **39,** 46–54
52. Silva, P. J., and Ramos, M. J. (2005) *J. Phys. Chem. B.* **109,** 18195–18200
53. Silva, P. J., Schulz, C., Jahn, D., Jahn, M., and Ramos, M. J. (2010) *J. Phys. Chem. B.* **114,** 8994–9001
54. Steiner, E. C., and Gilbert, J. M. (1963) *J. Am. Chem. Soc.* **85,** 3054–3055
55. Lovell, S. C., Word, J. M., Richardson, J. S., and Richardson, D. C. (2000) *Proteins* **40,** 389–408